Research in Astronomy and Astrophysics, 25:015016 (11pp), 2025 January

https://doi.org/10.1088/1674-4527/ad9da3
CSTR: 32081.14.RAA.ad9da3

# New Orbital Parameters of 850 Wide Visual Binary Stars and Their Statistical Properties

Igor Izmailov and Maxim Khovritchev
Central Astronomical Observatory, Russian Academy of Sciences, 65/1 Pulkovskoye Chaussee, St. Petersburg, 196140, Russia; i_izmailov@mail.ru
*Received 2024 November 05; revised 2024 December 03; accepted 2024 December 10; published 2025 January 13*

## Abstract

Based on positional observations and measurements of radial velocities, the orbits of 850 wide visual binary stars have been determined. The parameters of the log-normal distributions for the histograms of orbital periods, stellar masses, and semimajor axes in astronomical units have been obtained. The eccentricity histogram for binary stars with orbital periods less than 400 yr follows a normal distribution centered at $e = 0.545 +/- 0.029$. For stars with longer periods, this distribution obeys the law $f = 2e$, with accuracy to errors. The mass-to-luminosity relation for stars with well-determined masses is given by: $\log L_{\odot} = 4.33 \log \mathfrak{M}_{\odot} - 0.11$, where $L_{\odot}$ and $\mathfrak{M}_{\odot}$ are the luminosity and mass of the star in units of the solar luminosity and mass, respectively.

*Key words:* (stars:) binaries: visual – stars: statistics – stars: fundamental parameters

## 1. Introduction

The United States Naval Observatory maintains a comprehensive and continuously updated catalog (Mason et al. 2001) of visual double stars, which currently contains over 154,000 records. However, as outlined in the Sixth Catalog of Orbits, approximately 3500 binary star orbits have been determined (Hartkopf et al. 2001). Additionally, the orbits have been determined by various authors using various methods. This complicates the data application for different investigations such as orbital parameter distribution analysis for a certain sample of the stellar population.

The catalog categorizes all orbits into five grades, from 1 (definitive) to 5 (indeterminate). Initially, the grade assignment happened with a significant subjective element (Worley & Heintz 1983). However, for now, a well-formalized technique is used. It is based on the convergence between positional observation data and ephemerides calculated using orbital elements. Additionally, the coverage of a visible ellipse by observational data should be taken into account. The short observational series duration compared to the orbital period value results in considerable uncertainties in estimating the orbital elements, even with highly precise data.

Formal application of the orbital element standard error estimates in statistical treatments may distort the conclusions due to the peculiarities of the computing approaches. For example, the same observational data set may give quite different standard error values for two different techniques. This inhomogeneity in used approaches of the orbital element determinations guarantees the incorrectness in conclusions since the statistical weights are based on the error estimates.

The usage of the difference in the radial velocity between the components derived through spectroscopic observations significantly decreases the orbital parameter uncertainty for long-period binaries. It is reasonable to apply the method of apparent motion parameters (AMP; Kiselev & Kiyaeva 1980) for this case. The recent improvements in the radial velocity determination technique in the context of exoplanet research allow astronomers to decrease the radial velocity standard errors and to detect the relative radial accelerations of the binary components.

Moreover, Gaia catalog astrometric data (positions and proper motions) are available for both components of the most visual double stars (Gaia Collaboration et al. 2023). Gaia data turned out to be valuable for orbital solutions thanks to their high accuracy concerning ground-based measurements despite giving just one measurement on the visible ellipse and in the velocity space. The significance of the binary star investigation is that these objects hold valuable information about the genesis of the stellar population, which is partially preserved in their kinematics and statistics. During the fragmentation of a protostellar cloud, various configurations of closely spaced stars can emerge, as they tend to form within a common gravitational potential well. Binary systems, in particular, are known to be among the most stable configurations.

Analyzing the statistical parameters of binary star samples can enhance our understanding of the fragmentation process in protostellar clouds and the subsequent evolution of stellar populations. Investigation of the long-period binary stars is especially significant. A relatively short orbital period means a relatively short distance between the components during the early stages of their evolution. Therefore, the neighboring

objects that form simultaneously would have less influence on the binary being considered.

In this paper, we aimed to construct a comprehensive set of orbits of visual binary stars using a general technique for all objects. We relied on additional data regarding radial velocities, radial accelerations, precise positions, and proper motions obtained from the Gaia catalog. Furthermore, we propose to use the sets of possible orbits for each binary star instead of the orbit grades or the error estimates of the orbital elements.

## 2. Data Sample Formation

We compiled a list of 850 visual binary stars to perform a new determination of their orbital parameters. All of these binary stars meet several requirements. First, the separation between components must be greater than $0''.33$. Second, the positional observations should cover a significant arc of the orbit. Third, there was a considerable amount of current positional data on the level of accuracy of several milliarcseconds (mas) that have not been used before for orbital parameter determinations of stars. These data have been obtained through ground-based (speckle and CCD) observations, available from the Gaia or Hipparcos databases. A part of them resulted from astrometric observations (Izmailov et al. 2020) conducted with the Pulkovo 26 inch refractor ($D = 65$ cm, $F = 10.5$ m) equipped with FLI ProLine09000 CCD camera (field of view (FOV) $= 12' \times 12'$, scale $= 238$ mas pix$^{-1}$).

The orbital elements of 745 stars in our sample are listed in the Catalog of Orbits and Ephemerides of Visual Binary Stars (Hartkopf et al. 2001). Many of these stars have a rich observational history. As noted in our third criterion, new highly accurate data for these stars (Pulkovo data, space-based, and speckle-interferometric measurements) are available. Therefore, refining the orbital elements is a logical next step. A significant portion of the raw positional data was obtained from the Washington Double Star database (WDS), provided by Rachel Matson upon our request.

## 3. Orbital Parameter Determination Technique

### 3.1. The General Notes on the Computation of the Orbital Elements

There are many possible ways to construct the orbital parameter determination technique. In most cases, the algorithms are based on the well-known Equations (1) describing a transformation from the coordinates in the orbital plane coordinate system $X$, $Y$ to the $x$, $y$-coordinates in the sky plane.

$$\begin{aligned} x &= A \cdot X + F \cdot Y \\ y &= B \cdot X + G \cdot Y. \end{aligned} \tag{1}$$

The Thiele-Innes elements, $A$, $B$, $F$, and $G$, can be expressed as functions of the semimajor axis and the Campbell elements ($i$, $\omega$, $\Omega$) that fix the orbital plane orientation relative to the sky plane. The corresponding formulas are met in almost every paper regarding the determination of the orbital elements from van den Bos (2016) to Halbwachs et al. (2022).

The Equations (1) are linear with respect to $A$, $B$, $F$, and $G$. Accordingly, the standard least squares approach is applied to calculate Thiele-Innes elements using astrometric $x$, $y$-measurements. Thus basically, the differences between diverse techniques come from the way of eccentricity, orbital period, and periastron epoch ($e$, $P$, $T$) estimation required to calculate $X$, $Y$. This depends on the observational data properties (e.g., orbit coverage by observations) and computational resource limits. For example, the Gaia team used Markov Chain Monte Carlo (MCMC) and Genetic Algorithm (Holl et al. 2022). For the wide stellar pairs with a relatively large orbital period, the Gaia and/or Hipparcos proper motion and radial velocity differences between the components of the binary system are taken into account (Pearce et al. 2020). The Bayesian rejection-sampling algorithm has been applied to compute posterior distributions of orbital elements (Blunt et al. 2017). The authors demonstrate the advantages of their technique in comparison to the MCMC-based approach.

### 3.2. Brief Analysis of Our Data Set

The basic part of our source data is the time series of angular separation and positional angle ($\rho$, $\theta$) that came from ground-based astrometric observations. The $x$, $y$-coordinates were calculated with well-known expressions $x = \rho \cos\theta$, $y = \rho \sin\theta$. The accuracy of these positional data ranges from several mas (current CCD or speckle-interferometric observations) to about a hundred mas (old photographic observations).

The high-accuracy relative coordinates and proper motions from the Hipparcos and Gaia catalogs are now available for most of our stars. These data correspond to one or two $x$, $y$ dots on the trajectory but play a significant role because of the low level of standard errors (about 0.01–1 mas and 0.1–1 mas yr$^{-1}$). Furthermore, we utilized the available relative radial velocities from Gaia Data Release 3 (DR3) or other sources.

### 3.3. The Distinctive Features of Our Technique of Computation of the Orbital Elements Based on the Thiele-Innes Approach

Our pipeline for calculating the orbital elements is based on the properties of the data. We used $x$, $y$-data discussed before. They are mostly the results of ground-based astrometric observations covering a considerable part of the orbit. Therefore, our procedure includes the following stages.

1. We preferred not to apply the Markov Chain-based minimization algorithms. Indeed, it is easy to form a grid of $e$, $P$, $T$-triplets that covers all considered space with a certain step. In our case, there were 6000 triplets. Then we solve Equation (1) for all triplets. This is very fast due to the linearity of Equation (1). For every triplet, we calculated the Residual Sum of Squares (RSS). This sum characterized the quality of the approximation and was calculated according to RSS $= r^T r$, where $r$ is a column vector formed by the concatenation of $x - (A \cdot X + F \cdot Y)$ and $y - (B \cdot X + G \cdot Y)$ vectors. Finally, we chose ten triplets with the smallest RSS values for further calculations.
2. Each of these ten triplets is used as the initial values for further improvements of the corresponding $e$, $P$, and $T$. The residuals $\Delta x = x - (A \cdot X(e, P, T) + F \cdot Y(e, P, T))$ and $\Delta y = y - (B \cdot X(e, P, T) + G \cdot Y(e, P, T))$ were expressed using linear Equations (2) with respect to the corrections $\Delta e$, $\Delta P$, and $\Delta T$.

$$\begin{aligned} \Delta x &= \frac{dx}{de}\Delta e + \frac{dx}{dP}\Delta P + \frac{dx}{dT}\Delta T \\ \Delta y &= \frac{dy}{de}\Delta e + \frac{dy}{dP}\Delta P + \frac{dy}{dT}\Delta T. \end{aligned} \quad (2)$$

These equations were solved iteratively. The new $e$, $P$, and $T$ values for the $n$th iteration were calculated using formulas (3), where $\lambda > 0$ is the regularization factor. The condition for choosing the $\lambda$ value was decreasing the RSS value. The initial value of $\lambda$ was consecutively decreased while $\mathrm{RSS}_n \geqslant \mathrm{RSS}_{n-1}$ and increased for the other case.

$$\begin{aligned} e_n &= e_{n-1} + \lambda \Delta e \\ P_n &= P_{n-1} + \lambda \Delta P \\ T_n &= T_{n-1} + \lambda \Delta T. \end{aligned} \quad (3)$$

The threshold value for $\lambda$ was set at $10^{-10}$. If the $\lambda$ value reached this limit, an attempt was made to assign random values for $\Delta e$, $\Delta P$, and $\Delta T$. The calculations were finished if this attempt was unsuccessful. These iterations were interrupted when $\Delta e \approx P \approx \Delta T \approx 0$.
3. The solution with the lowest RSS value among these ten solutions was selected as the final result.

It is natural that every source $\rho$, $\theta$ data set consists of the subsets of measurement results taken at different observatories with diverse accuracy. The measurements taken from space are significantly more accurate than those from the ground, being 10–100 times better. Therefore, it makes sense to assign weights to each subset of observations. This issue has been examined in numerous papers (e.g., Mendez et al. 2017 and Anguita-Aguero et al. 2022). Their authors outlined that the procedure of assignment of weights is often somewhat subjective. The idea to calculate weights according to the telescope parameters (focal lengths and apertures) became invalid. For instance, it has been shown that there are no significant differences between astrometric accuracy estimates reached with the Pulkovo 26 inch refractor and the 4 meter telescope for the same binaries (Izmailov et al. 2020). Thus, we developed the procedure of weight calculation based on the positional differences between the set of observations conducted by a specific observatory and the ephemerides provided by the "etalon set of orbital elements."

1. For pairs with periods greater than 500 yr, we calculate "etalon orbits" using median coordinates derived from 19th-century observations, Hipparcos positions, Gaia positions, and proper motions.
2. The $x$, $y$ residuals concerning these "etalon orbits" were computed for all individual observatory data sets.
3. The standard deviations have been calculated for all observatories with more than ten residuals. The corresponding weights were assigned as inverse squares of these standard deviations.
4. All observatories with a number of residuals less than ten were collected in one group with the value of weight calculated according to the corresponding residuals.

The homogeneous coordinate subsets taken by the same observatory were used to reduce the calculation complexity. For each of them, we form the normal place, i.e., coordinates and values of relative velocities at the mean epoch. These data were used for the orbit calculation. The equations incorporating velocity values are straightforward. We replace the coordinates with their time derivatives in Equations (1).

### *3.4. The Application of the Apparent Motion Parameters Technique for the Improvement of the Values of the Orbital Parameters*

We have radial velocities and estimates of radial acceleration for a sample of stars in our data set. AMP is a technique that allows us to consider these data. AMP was developed at Pulkovo Observatory (Kiselev & Kiyaeva 1980). This method is primarily used for determining binary star orbits when astrometric observations cover only a short arc of the trajectory.

The natural units for values in the AMP equations are astronomical units (au) and au $\mathrm{yr}^{-1}$ for the spatial coordinates, distances, and velocities; years for the time intervals (e.g., orbital periods); and solar masses for the masses of the primary and secondary components of the binary system ($\mathfrak{M}_p$, $\mathfrak{M}_s$).

Astrometric observation results can be represented as a set of angular separations between the components of a binary system, with positional angles denoted as $\rho(t_i)$ and $\theta(t_i)$. Here, $t_i$ (where $i = 0, \ldots, N$) represents the moments of time corresponding to each observation, and $N$ is the total number of observations. For a

short arc of observations, these series can be approximated using a linear model: $\rho(t_i) = \rho_0 + \dot{\rho}(t_i - t_0)$, $\theta(t_i) = \theta_0 + \dot{\theta}(t_i - t_0)$. In this model, $\rho_0$ and $\theta_0$ can be derived using the linear least squares method at the mean epoch of observations ($t_0$).

The relative proper motion is defined by two values. These are the absolute value of the proper motion $\mu = \sqrt{\dot{\rho}_0^2 + (\rho_0\dot{\theta})^2}$ and the corresponding positional angle $\psi$.

The value of the local curvature of the relative trajectory $\rho_c$ is equal to the radius of the circle that optimally represents the observed relative motion.

The basic equation of the AMP technique can be expressed as follows

$$r_0^3 = \left(\frac{k^2}{\mu^2}\right)\rho_0\rho_c \sin(\psi - \theta_0). \quad (4)$$

Here $r_0$ is a spatial distance between the components of the binary system at the mean epoch $t_0$, and $k^2 = 4\pi^2(\mathfrak{M}_p + \mathfrak{M}_s)$.

Equation (4) allows us to estimate the distance between the primary and secondary at epoch $t_0$. This is possible due to the availability of high-quality parallax and photometric measurements from Gaia. The a priori mass estimations rely on modern isochrones, metallicity, and interstellar extinction data (e.g., Kiyaeva et al. 2021).

Hence, the $z_0$ value can be computed as $\pm\sqrt{r_0^2 - \rho_0^2}$. The complete set of kinematic data ($x_0$, $y_0$, $z_0$, $\dot{x}_0$, $\dot{y}_0$, $\dot{z}_0$) and the sum of the masses $\mathfrak{M}_p + \mathfrak{M}_s$ can easily be transformed into the seven orbital elements. Therefore, having the relative radial velocity $\dot{z}_0$ obtained from the observations provides the final element needed to complete the kinematic data set.

It is important to note that the technique described does not provide a system of orbital elements based on all available data when there is good orbital coverage. However, it allows us to have a good initial approximation, which can be further refined using the Thiele-Innes method. In this case, we can avoid the procedures based on MCMC that were discussed above.

Recent spectroscopic observations of bright double stars have provided measurements of their relative radial velocities over the past few decades. These measurements include radial velocities from several epochs for a sample of binary stars. This allows us to calculate the values of relative radial acceleration using the formula $W = \Delta\dot{z}/\Delta t$. The expression for $W$ can be written in terms of the AMP according to Newton's law of gravitation (5).

$$W = -\frac{k^2}{r_0^3}z_0. \quad (5)$$

The combination of Equations (4) and (5) gives us the $z_0$ estimate that is independent of the sum of stellar masses (6).

$$z_0 = \pm\frac{1}{\mu^2}W\rho_0\rho_c \sin(\psi - \theta_0). \quad (6)$$

Therefore, it is logical to use $\dot{z}_0$ and $W$ in the procedure of orbital elements calculation for the corresponding binary stars.

1. A preliminary set of orbital parameters was calculated through the Thiele-Innes procedure using all positional data. The mean values of $\rho$, $\theta$, and $\mu$ with the corresponding standard errors were computed for a separate series of observations obtained from the single telescope observations. Single observations of $\rho$, $\theta$ were used as independent points. The relative positions and proper motions from Gaia were taken into account. Weights were assigned according to the standard errors.
2. The AMP elements $\rho_0$, $\theta_0$, $\mu$, $\psi$, $\rho_c$, and $\dot{z}$, $W$ were calculated at the epoch of radial velocity determination using the elements of the preliminary orbit.
3. The values $\dot{z}$, $W$ from the previous stage were substituted for the observed ones. Then, orbital elements were recalculated using a new set of AMP parameters.
4. The improvement of five elements $\rho_0$, $\theta_0$, $\mu$, $\psi$, $\rho_c$ was performed with a nonlinear least squares procedure using the complete set of positional data taking weights into account. Partial derivatives were computed numerically. If $W$ was not available, the $k^2$ value was added and improved in a similar manner.

### 3.5. The Types of Orbital Solutions

In previous sections, the technique for determining orbital elements was briefly described. The calculation procedure takes into account the types and quality of observational data for each binary star in our sample. As a result, the systems of orbital solutions for different binaries are statistically unequal. This should be considered when using the presented data. Consequently, the obtained orbital solutions are classified into the following types.

*Solution 1*. Binary systems for which only ground-based astrometric measurements were available. For these stars, we applied our modification of the Thiele-Innes approach.

*Solution 2*. Stellar pairs that have both Hipparcos and Gaia data (relative position and proper motion) in addition to ground-based astrometric measurements. A method similar to the previous solution was applied. The weights were assigned to the data according to their standard errors including space-based data.

*Solution 3*. The measurements of radial velocity for these stars are available. The solution was obtained using the AMP technique as described above.

*Solution 4*. The radial velocities and radial accelerations of these stars are available. The AMP algorithm branch based on Equation (6) was used.

The quality of the solutions generally improved from Solution 1 to Solution 4 due to the incorporation of new

high-accuracy data. However, there were instances where this pattern was not met. In such cases, we selected the solution with the minimum standard errors as the final result. For example, a formal advantage of Solution 1 over Solution 2 could arise from the presence of an unknown third companion in the binary system, which would have perturbed the relative motion determined by the orbital parameters calculated in Solution 1.

In Tal-Or et al. (2019), the radial accelerations for seven pairs of stars are given:

1. WDS 00057+4549 AB = ADS 48,
2. WDS 00184+4401 AB,
3. WDS 00491+5749 AB,
4. WDS 16133+1332 AB,
5. WDS 18428+5938 AB = ADS 11632,
6. WDS 19121+4951 AB,
7. WDS 21069+3845 AB = 61 Cyg.

61 Cyg is a binary system with a rich history, discussed in over 100 research papers. We conducted a separate study on this object (Izmailov & Apetyan 2024). Unfortunately, for WDS 00491+5749 AB, while radial acceleration has been measured, there is no reliable measurement of radial velocity. Therefore, we have determined the orbit using the Thiele-Innes method. For the remaining five stars, the orbit determination based on acceleration significantly improved the accuracy of the orbital elements and the total masses of the components. For WDS 00057+4549, also known as ADS 48, the sum of the masses is given in solar masses.

1. by the Thiele-Innes method $1.859 \pm 2.025$,
2. by the Thiele-Innes method, using Gaia data $1.639 \pm 1.192$,
3. by the AMP method $1.294 \pm 1.245$,
4. by the AMP method, using a radial acceleration $1.304 \pm 0.061$.

The errors in the orbital elements were calculated similarly to the method described in the previous paper Izmailov (2019). First, we calculated ephemeris positions from the obtained orbit for all observation moments. Then, we added model random noise, with a standard error derived from the main orbit determination, to these ephemeris positions. Additionally, model noise was incorporated into the radial velocity and radial acceleration for orbits calculated using these parameters. We then re-determined the orbit based on these model data and repeated this calculation 100 times.

As a result, for each pair of stars, we obtained a set of 100 orbits that described an area of possible orbital solutions. We sorted the arrays of 100 values for all elements, including mass, and determined the size of the interval that contains 68.27% of all estimates. Interpolation was applied to obtain the precise value of 68.27%. It is important to note that the value of 68.27% corresponds to the probability of finding a random value within the $\pm\sigma$ interval for normal random values.

We present the complete set of 100 possible orbits, containing one corresponding to the minimum rms value. It is important to note that the orbit with the minimum rms is not necessarily located at the center of the area of possible orbital solutions. From our point of view, this coincidence (the orbit with the minimal rms aligns with the center of the region) happens primarily for the orbit that is well-conditioned, for example, in case the entire visible ellipse is well-covered by observations.

Furthermore, in general cases, this center may lie outside the area due to the non-convex cross-sectional shape. This statement has been validated with our data. The orbit identified as the center of the region corresponds to the average median values derived from the 100 orbit solutions. Naturally, this central orbit is only one orbit from the region if its rms is less than the maximum rms of the original set of orbits. The center of possible orbital solutions lies outside this area for 540 cases of 850 pairs.

The representation of an orbit using elements with standard errors generally assumes that the shape of the region of possible orbital solutions forms an ellipsoid in a seven-dimensional space. In this representation, the axes of the ellipsoid align with the coordinate axes.

Alternatively, a representation can include paired covariations. This is similar to covariance matrix elements for five-parametric solutions in the Hipparcos and Gaia catalogs. This suggests an error ellipsoid with axes that can be oriented arbitrarily. Considered regions for the binary orbital elements can have diverse shapes. While studying the properties of these forms would be theoretically interesting, a simpler approach is to utilize sets of orbits whenever uncertainty estimates for the elements are required.

For instance, instead of calculating the mass of a binary system based on a single central orbit and then deriving the error estimate using an error propagation expression, we can calculate the mass as the median mass from a set of 100 orbits. The "standard error" is then estimated from the same set of calculated masses.

The star system designated as WDS 03520+0632 = 31 Tau may be presented as an illustration of the advantages of our approach. It is the most massive system with a reliably defined mass in our analysis. Observations of this binary star were conducted from 1937 to 2019. During this period, the positional angle changed from $215^{\circ}.0$ to $206^{\circ}.9$, and the distance between the components varied from $0''.3$ to $0''.8$, indicating that only a relatively small arc of the orbit was covered.

The primary star is classified as B5V, and the lack of narrow absorption lines in its spectrum prevents us from obtaining accurate estimates of both radial velocities and accelerations. At first glance, it may appear that determining orbital elements

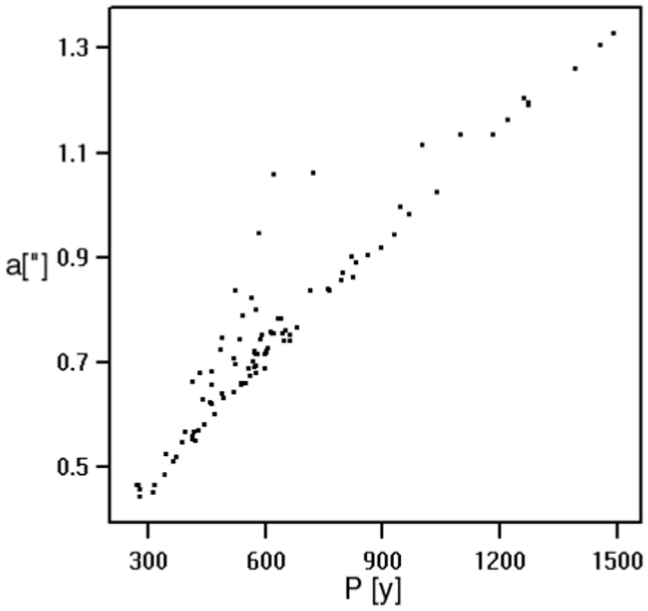


**Figure 1.** The relationship between the period and semimajor axes of possible orbits for the binary star system 31 Tau.

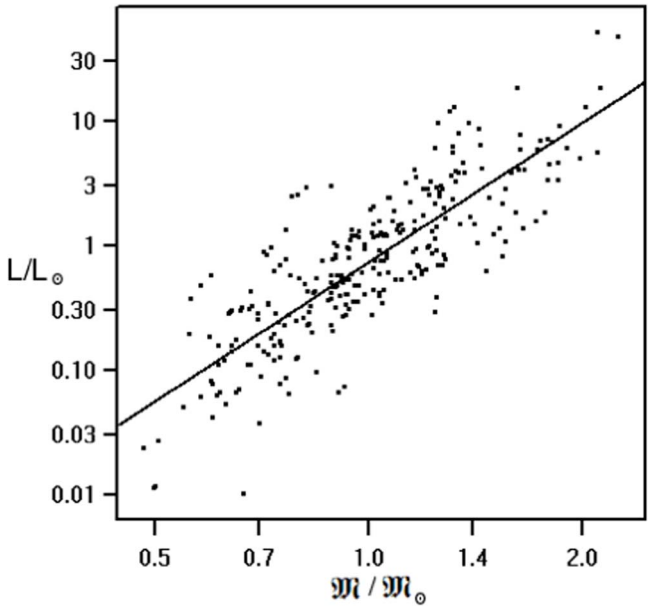


**Figure 2.** The mass–luminosity ratio for 850 binary stars studied in this paper.

and masses is impossible. Fortunately, there is a strong correlation between the orbital period and the semimajor axis in the potential orbits of this binary system (see Figure 1). Consequently, the mass dispersion derived from different possible orbits is less than the dispersion in semimajor axes and periods. Taking parallax error into account, the total mass of the components of this star system is estimated to be $12.3^{+3.4}_{-1.3}$ solar masses.

Another example of a potential application of our technique involves a pair of celestial bodies within a group of relatively close objects with similar masses. In this scenario, *N*-body simulations are essential to investigate the dynamical evolution of the system. This analysis could be particularly useful for studying the orbit evolution of exoplanets in binary systems or the dynamical evolution of stellar clusters. In such cases, separate numerical integrations for each orbit in the set are necessary.

## 4. The Results

The primary outcome of this study is the orbital solutions for 850 visual binary stars. The associated data are presented in four tables, which can be accessed as ASCII files through the Pulkovo Observatory database (http://izmccd.puldb.ru/vds.htm) or the Strasbourg astronomical Data Center (CDS) (https://cds.u-strasbg.fr).

1. *Table 1*. This table presents the sums of masses of the components for 184 stellar pairs, measured in solar masses.
2. *Table 2*. This table includes the sums of the component masses of 850 stars, each multiplied by the cube of their parallax.
3. *Table 3*. Here, the orbital elements for the solution with the minimum rms are provided for all binaries in our sample.
4. *Table 4*. Each entry in this table contains 100 orbits for each binary star, outlining the range of possible orbital solutions as described above.

Table 1 also provides the lower and upper bounds of the confidence interval for the sum of stellar masses calculated with a probability of 0.6827. Only pairs for which the sum of the mass estimate is three times greater than half of the confidence interval are included. Out of 850 pairs, 184 meet this condition. The corresponding parallax data were taken from the Gaia DR3 catalog. Additionally, since stellar magnitude and interstellar absorption are also determined by Gaia, the mass–luminosity relationship can be constructed for our sample. It is shown in Figure 2.

$$\log \frac{L}{L_\odot} = a \cdot \log \frac{\mathfrak{M}}{\mathfrak{M}_\odot} + b. \tag{7}$$

Here $\frac{L}{L_\odot}$ is the luminosity in solar units, in the *G* band, and $\frac{\mathfrak{M}}{\mathfrak{M}_\odot}$ is the mass in solar masses.

Each binary pair in this figure is represented by two dots, meaning one star corresponds to one data point. The individual masses of the components were determined through a simple iterative procedure based on the mass–luminosity law. The mass

ratio for a pair of stars was derived from this law, and the individual masses were calculated using a known sum of masses.

In the iterative process, we initially set $a = 4$ and $b = 0$. Using these values, we calculated the individual masses, then updated $a$ and $b$ based on the computed masses. This process continued until the values converged and stabilized. The results we obtained are as follows

$$a = 4.33 \pm 0.15$$
$$b = -0.11 \pm 0.14. \quad (8)$$

In the paper of Eker et al. (2018), the values of $a = 4.329 \pm 0.087$ and $b = 0.010 \pm 0.019$ for eclipsing variable stars of the average mass range are presented. They agree with our values within standard errors.

Similar to the previous, we can calculate absolute magnitude $M_G$ in the $G$ band according to

$$M_G = -10.82\{\pm 0.37\} \cdot \log \frac{\mathfrak{M}}{\mathfrak{M}_\odot} + 4.901\{\pm 0.048\}. \quad (9)$$

A theoretical estimate was produced by Malkov et al. (2022) for slightly more massive stars with a mass of $1.4 < \frac{\mathfrak{M}}{\mathfrak{M}_\odot} < 2.27$

$$M_G = -9.53 \cdot \log \frac{\mathfrak{M}}{\mathfrak{M}_\odot} + 4.33, \quad (10)$$

which is also close to our results, although it is out of the $1-\sigma$ error interval.

The noticeable dispersion in the data points relative to the straight line is likely due to the different ages and metallicities of the stars. It is essential to create a set of evolutionary tracks based on the metallicity and color of the stars, allowing us to select the appropriate track for each star (see Bressan et al. 2012) to conduct a more detailed analysis. The authors intend to continue this research in the future.

A histogram displaying the distribution of the 850 studied binary stars by their eccentricities is shown in Figure 3. For this analysis, all 100 orbital solutions for each binary star were utilized. It is also evident from the figure that the histogram exhibits a slight upward deviation from the linear law represented by the equation $f(e) = 2e$.

Figure 4 illustrates the histogram for eccentricities, focusing only on orbits for which the eccentricity standard error is less than 0.1 and the period is under 400 yr. In contrast, Figure 5 presents orbits with a period exceeding 400 yr, applying the same criterion regarding the eccentricity error.

Unfortunately, only 85 orbits fall within this short-period set ($P < 400$ yr). The peak of this histogram corresponds to an eccentricity of $e = 0.545 \pm 0.029$. This estimate, like all subsequent ones, is derived by approximating the data points using a normal distribution. In the paper by Tokovinin & Kiyaeva (2016), similar calculations were based on a sample of 477 close binary stars, which did not have direct orbit determinations. The corresponding peak of the histogram of

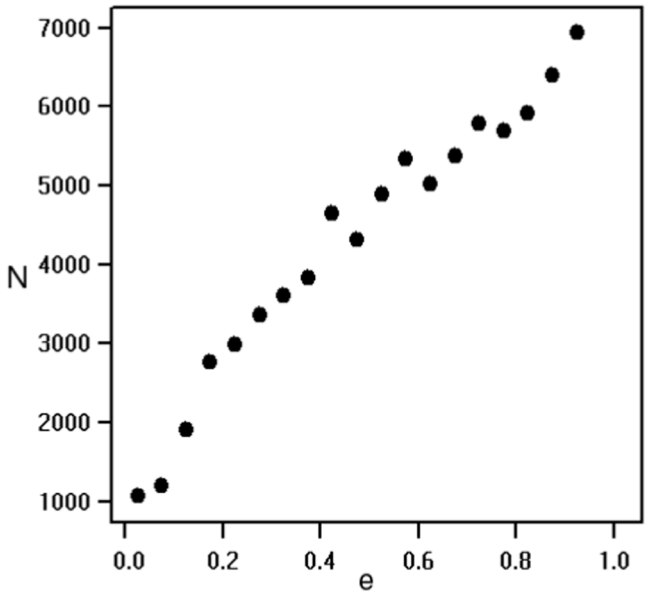


**Figure 3.** A histogram of all 850 binary stars by eccentricities.

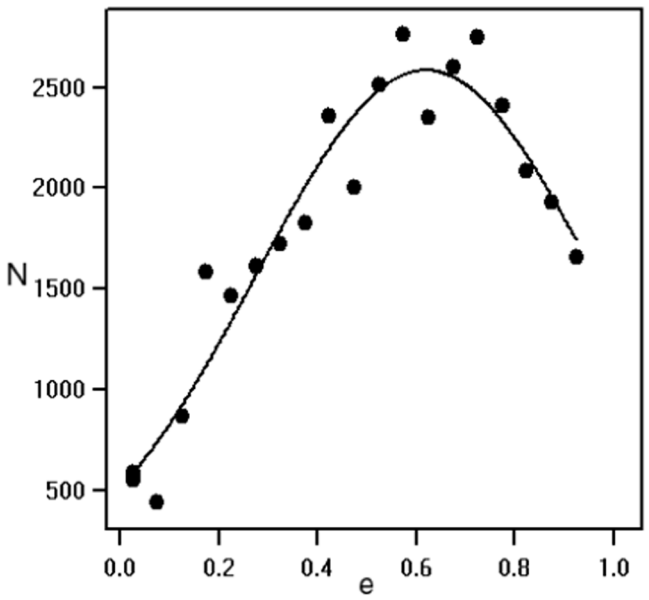


**Figure 4.** A histogram of binary stars by eccentricity, with periods less than 400 yr, and with an eccentricity error of less than 0.1.

$0.59 \pm 0.02$ was determined. This is within $2\sigma$ agreement with our result. The paper also notes that this maximum tends to shift upward with an increase in the orbital period. Furthermore, in Marks & Kroupa (2011), which updated the statistics obtained from the radial velocities of 164 Sun-like stars in Duquennoy & Mayor (1991), it was shown that the distribution law $f(e) = 2e$ accurately describes the analyzed data.

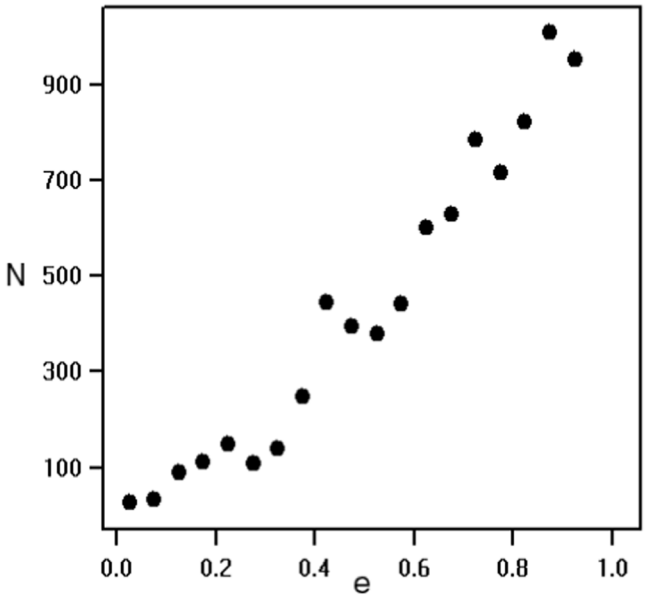


**Figure 5.** A histogram of binary stars by eccentricity for orbital periods greater than 400 yr and with an eccentricity error of less than 0.1.

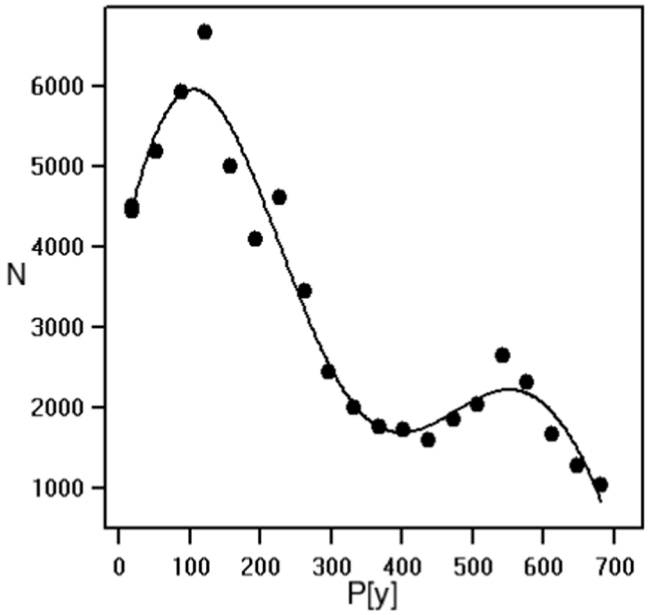


**Figure 6.** A histogram of binary stars by period for our sample.

Without limiting the eccentricity error, the histogram of the eccentricity shows the ratio of stars with periods longer than 400 yr in our sample.

$$f(e) = -0.033\{\pm 0.087\} + 2.07\{\pm 0.16\}e, \qquad (11)$$

which also confirms the $f(e) = 2e$ law within standard error limits.

Figure 6 shows a histogram by period.

It is unfortunately not feasible to impose a limitation on period errors, as was done for eccentricities. Such a restriction would reduce the sample of binary stars with long periods since the period value directly affects its relative error. This is explained by relatively poor orbit coverage by observations for the binary stars with relatively big orbital periods. In comparison to the previous study Izmailov (2019), a bimodal pattern in the distribution has been confirmed. However, the first maximum has shifted toward shorter periods from 200 to 87 yr. The exact position of this first maximum remains quite uncertain. The second maximum was retained at $587 \pm 83$ yr. It is possible that the addition of a significant number of short-period binaries could shift the first maximum position even further, but the bimodal pattern of the distribution will likely persist. Interestingly, in the logarithmic scale (see Figure 7), the first maximum is still observed around the value $P = 208 \pm 73$.

The two peaks in the histogram nearly merge, making it possible to interpret the distribution as single-modal, with a maximum at $342 \pm 28$ yr. This finding is quite similar to the result reported in Raghavan et al. (2010), where a similar maximum is detected at $P = 293$ yr. The discussed bimodality in the distribution could lead from both the intrinsic properties

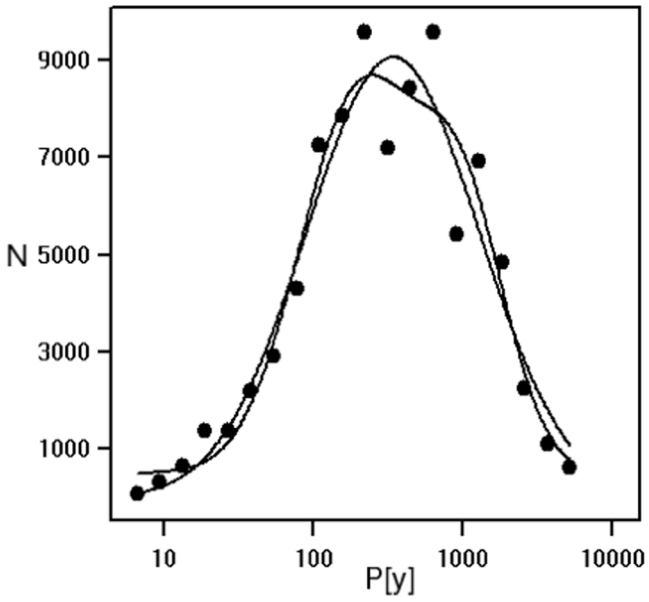


**Figure 7.** A histogram of the distribution of binary stars by their periods on a logarithmic scale.

of the stellar population and a combination of selection effects, limitations from observation intervals, and the limitations of methods used for orbit determinations. For instance, Offner et al. (2010) outlined two mechanisms for binary star formation. Here stars are selected for analysis only if the value of the major semimajor axis is at least three times greater than its standard error. The distribution is single-modal, with a

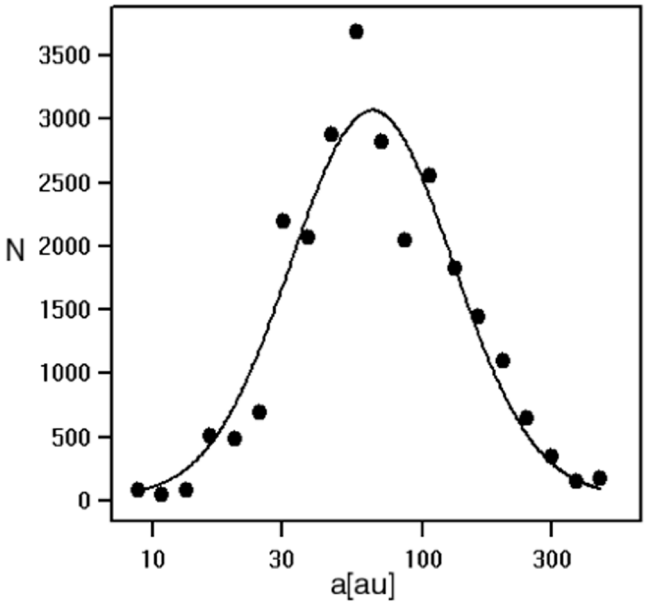


**Figure 8.** A histogram of the binary stars of our sample by semimajor axes on a logarithmic scale.

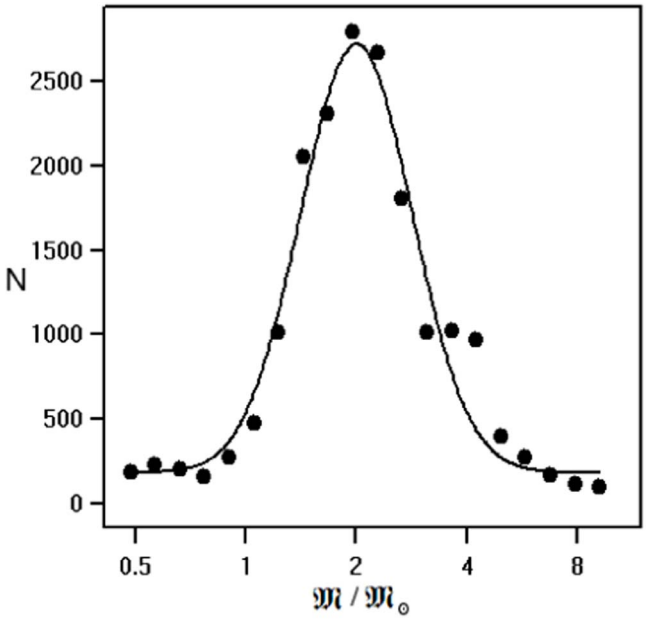


**Figure 9.** A histogram of binary stars by mass values.

maximum at $\log a[au] = 1.812 \pm 0.020$, which corresponds to 64.9 Astronomical Units (au). Since the distance to the binary (measured by parallax) was used to convert the size of the semimajor axis from angular seconds to astronomical units, it is possible to examine selection effects related to both distance and the apparent separation of components. The sample was divided into two equal groups based on distance: relatively close binaries to the Sun and located relatively far from the Sun. A similar division was made for the values of the semimajor axes. All distributions corresponding to these four subsets show a similar shape to the original distribution. This consistency allows us to infer that the distribution we obtained for the semimajor axis is more indicative of the stellar population's properties rather than the effects of selection. A histogram of the semimajor axes in the logarithmic scale is shown in Figure 8.

The distribution of binary stars by mass reaches its maximum at $\log \frac{\mathfrak{M}}{\mathfrak{M}_\odot} = 0.3016 \pm 0.0089$ for our sample. This corresponds to a mass ratio of $\frac{\mathfrak{M}}{\mathfrak{M}_\odot} = 2.00$ solar masses (see Figure 9). The mass represented here is the sum of the masses of two stars, with one of the stars having a mass approximately

**Table 1**
The Parameters of Distribution Fittings by the Normal Low for Some Orbital Elements

| Name Of the orbital element | Features of the solution | Element | Position of the maximum | $\sigma$ (standard deviation of normal distribution) |
|---|---|---|---|---|
| eccentricity | $P <$ 400 yr | $e$ | 0.545 | 0.350 |
| ... | ... | ... | ±0.029 | ±0.018 |
| ... | | | | |
| logarithm of | ... | $\log a$ | 1.812 | 0.299 |
| semimajor | ... | ... | ±0.020 | ±0.033 |
| axis (a.u.) | ... | ... | ... | ... |
| ... | | | | |
| logarithm of | ... | $\log \frac{\mathfrak{M}}{\mathfrak{M}_\odot}$ | 0.3016 | 0.153 |
| mass in solar masses | ... | ... | ±0.0089 | ±0.011 |
| ... | ... | ... | ... | ... |
| ... | | | | |
| logarithm of | solution | $\log P$ | 2.534 | 0.606 |
| period (yr) | with one | ... | ±0.033 | ±0.069 |
| ... | maximum | ... | ... | ... |
| ... | | | | |
| logarithm of | solution | $\log P$ | ... | ... |
| period (yr) | with two | ... | ... | ... |
| ... | maximums | ... | ... | ... |
| ... | 1st maximum | ... | 2.313 | 0.401 |
| ... | ... | ... | ±0.196 | ±0.123 |
| ... | 2st maximum | ... | 3.120 | 0.397 |
| ... | ... | ... | ±0.190 | ±0.125 |
| ... | | | | |
| period (yr) | solution | $P$ | ... | ... |
| ... | with two | ... | ... | ... |
| ... | maximums | ... | ... | ... |
| ... | 1st maximum | ... | 87 | 154 |
| ... | ... | ... | ±101 | ±34 |
| ... | 2st maximum | ... | 587 | 267 |
| ... | ... | ... | ±83 | ±248 |

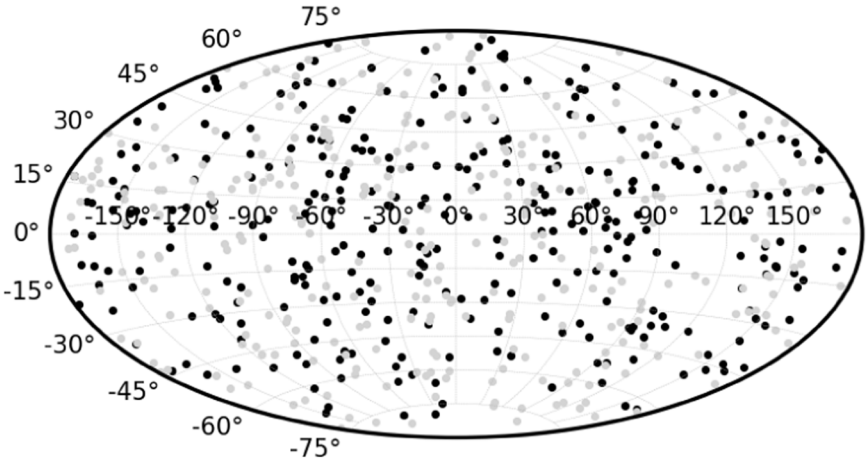


**Figure 10.** The distribution of poles of 324 binary orbits over the celestial sphere in galactic coordinates. The binary orbit pole position was calculated for each orbit from each set for the corresponding binary system. The figure shows the mean pole locations only for the stars for which 68% of the poles fall into the 10° circle. There are two poles for each binary due to the uncertainty of the ascending node position (Ω is in black and Ω + 180 deg is in gray).

equal to that of the Sun. Our sample of binary stars is likely lacking in low-mass stars, and the real peak of this distribution probably falls at lower mass values.

The parameters of fitting the above distributions are summarized in Table 1.

The distribution of the poles of our orbits over the celestial sphere was examined in this study. It is important to note that such investigations have a long history, as referenced in Dommanget (2014). The paper by Agati et al. (2015) highlights the concentration of poles near the galactic coordinates $l = 46°$ and $b = 37°$, based on 51 binary systems in the solar vicinity. However, the authors caution that the reality of the deviation from isotropy cannot be concluded with certainty.

It is noted that there are two equally probable pole positions for all binary systems that lack spectral data. In a given tangential plane, two hypothetical binary systems, which differ only in the position of their ascending nodes by 180°, will demonstrate identical motion. For real systems, however, one pole position is valid while the other is not. Furthermore, the distribution of incorrect pole positions will generally be random in a relatively big sample of binaries. These incorrect poles should appear like a random noise. This noise complicates the detection of the effect but does not make such detection impossible.

A straightforward calculation was conducted to analyze the distribution of orbital poles across the celestial sphere and to assess any potential violation of isotropy. Only binaries that had a reliably determined pole position were utilized (see Figure 10). The HEALPix equal-area pixelization method was applied (Hivon & Banday 2005). The pixel areas varied, covering values from $1/2$, $1/3$, $1/4$ … $1/40$ of the total celestial sphere area. The pixel with the highest number of poles was identified for each specified pixel area value. Subsequently, the probability of obtaining the same or a greater maximum for a particular pixel area was evaluated. A numerical simulation involving 1,000 random distributions was performed to achieve this. In 538 out of these 1,000 cases, the maximum number of simulated poles exceeded the number of real poles.

The analysis of the concentration of the pole close to a certain plane was performed in a similar manner. The spherical zones were used instead of the HEALPix pixels. The real pole distribution maximum was exceeded in 766 cases out of 1000.

Therefore, neither the concentration of the poles in a certain direction on a sphere nor in a plane can be confirmed.

## Conclusion

Coordinates, proper motions, and corresponding standard errors from Gaia data were used in the orbit determination of the selected stars. These data were introduced into orbital solutions with the highest weight values thanks to the high accuracy of the Gaia astrometry compared to the ground-based data. Therefore, the ephemeris for the relative position of the components is close to the Gaia results at the mean Gaia epoch both in coordinates and in their standard errors. It is easy to calculate the accuracy of estimates of $\rho$, $\theta$ at the arbitrary epoch using orbit sets constructed for each binary. The initial step is computing the ephemeris $\rho_k$, $\theta_k$ for each orbit for the corresponding binary orbit set. Next, the mean value over the set of $\rho_k$, $\theta_k$ and their standard errors represent the ephemeris and the corresponding accuracy estimate of the relative position for the arbitrary epoch. The same procedure can be applied for the radial velocities and accelerations. The technique considered improves the accuracy of the ephemeris several times, in contrast to the standard method with error propagation.

Finally, we should note that our sample of the binary stars has significant selection biases from a statistical completeness point of view. There is a lack of binaries with low-mass components in the sample. The fraction of the low-mass component binaries should be significant in contrast to the

solar-mass component binary fraction for the complete sample of binaries. However, the low-mass component binaries have no long observation history due to their low brightness. As a result, the astronomical community focused heavily on these kinds of binary stars to collect sufficient astrometric data sets for accurate orbit determinations. Another limitation concerns the long-period binary stars. A relatively short observed arc leads to significant uncertainties in the orbital parameters. Hence, additional radial velocity and acceleration measurements will improve the orbital parameter convergence. Simultaneous astrometric observations of well-known bright binaries are necessary to refine current orbital parameter sets and potentially discover hidden low-mass components.

## Acknowledgments

This study has made use of data from the European Space Agency (ESA) mission Gaia,[1] processed by the Gaia Data Processing and Analysis Consortium[2] (DPAC). Funding for the DPAC has been provided by national institutions, in particular, the institutions participating in the Gaia Multilateral Agreement.

This research has made use of the Washington Double Star Catalog, maintained at the U.S. Naval Observatory, and the SIMBAD database, operated at CDS, Strasbourg, France.

The study was carried out with the financial support of the Russian Foundation for Basic Research under Contract No. 20-02-00563A.

## ORCID iDs

Igor Izmailov https://orcid.org/0000-0002-6064-6191

## References

Agati, J. L., Bonneau, D., Jorissen, A., et al. 2015, A&A, 574, A6
Anguita-Aguero, J., Mendez, R. A., Claverìa, R. M., & Costa, E. 2022, AJ, 163, 118
Blunt, S., Nielsen, E. L., De Rosa, R. J., et al. 2017, AJ, 153, 229
Bressan, A., Marigo, P., Girardi, L., et al. 2012, MNRAS, 427, 127
Dommanget, J. 2014, O&T, 83, 2
Duquennoy, A., & Mayor, M. 1991, A&A, 248, 485
Eker, Z., Bakış, V., Bilir, S., et al. 2018, MNRAS, 479, 5491
Gaia Collaboration, Vallenari, A., & Brown, A. G. A. 2023, A&A, 674, A1
Górski, K. M., Hivon, E., Banday, A. J., et al. 2005, ApJ, 622, 759
Halbwachs, J.-L., Pourbaix, D., Arenou, F., et al. 2022, arXiv:2206.05726
Hartkopf, W. I., Mason, B. D., & Worley, C. E. 2001, AJ, 122, 3472
Holl, B., Sozzetti, A., Sahlmann, J., et al. 2022, arXiv:2206.05439
Izmailov, I., Rublevsky, A., & Apetyan, A. 2020, AN, 341, 762
Izmailov, I. S. 2019, AstL, 45, 30
Izmailov, I. S., & Apetyan, A. A. 2024, AN, 345, e20230004
Kiselev, A. A., & Kiyaeva, O. V. 1980, AZh, 57, 1227
Kiyaeva, O. V., Khovritchev, M. Y., Kulikova, A. M., et al. 2021, RAA, 21, 291
Malkov, O., Kovaleva, D., Zhukov, A., & Dluzhnevskaya, O. 2022, Ap&SS, 367, 37
Marks, M., & Kroupa, P. 2011, MNRAS, 417, 1702
Mason, B. D., Wycoff, G. L., Hartkopf, W. I., Douglass, G. G., & Worley, C. E. 2001, AJ, 122, 3466
Mendez, R. A., Claveria, R. M., Orchard, M. E., & Silva, J. F. 2017, AJ, 154, 187
Offner, S. S. R., Kratter, K. M., Matzner, C. D., Krumholz, M. R., & Klein, R. I. 2010, ApJ, 725, 1485
Pearce, L. A., Kraus, A. L., Dupuy, T. J., et al. 2020, ApJ, 894, 115
Raghavan, D., McAlister, H. A., Henry, T. J., et al. 2010, ApJS, 190, 1
Tal-Or, L., Trifonov, T., Zucker, S., Mazeh, T., & Zechmeister, M. 2019, MNRAS, 484, L8
Tokovinin, A., & Kiyaeva, O. 2016, MNRAS, 456, 2070
van den Bos, W. H. 1926, CiUO, 68, 352
Worley, C. E., & Heintz, W. D. 1983, PUSNO, 24, 1

[1] https://www.cosmos.esa.int/gaia
[2] https://www.cosmos.esa.int/web/gaia/dpac/consortium